High-Order Shock-Fitting Solvers and Numerical Simulations of Hypersonic Non-Equilibrium Flows

Presented By

Xiaowen Wang

Assistant Professor

Aerospace Engineering and Mechanics

The University of Alabama, Tuscaloosa

Thermal & Fluids Analysis Workshop
TFAWS 2017
August 21-25, 2017
NASA Marshall Space Flight Center
Huntsville, AL

Outline

- **Introduction to high-order methods**
- **High-order shock-fitting method**
- **Application of the shock-fitting method to transition control using surface roughness**
- **More potential applications**
- **Summary**

What is a high-order numerical method?

- **A numerical method is said to be *k*-th order if the solution error *e* is proportional to the mesh size *h* to the power of *k***

$$\frac{dy}{dx} = f(x, y), Y_n' = f(nh, Y_n) \quad \Rightarrow \quad e = Y_n - y_n \propto h^k$$

- **A unanimous definition of high-order: third order or higher**

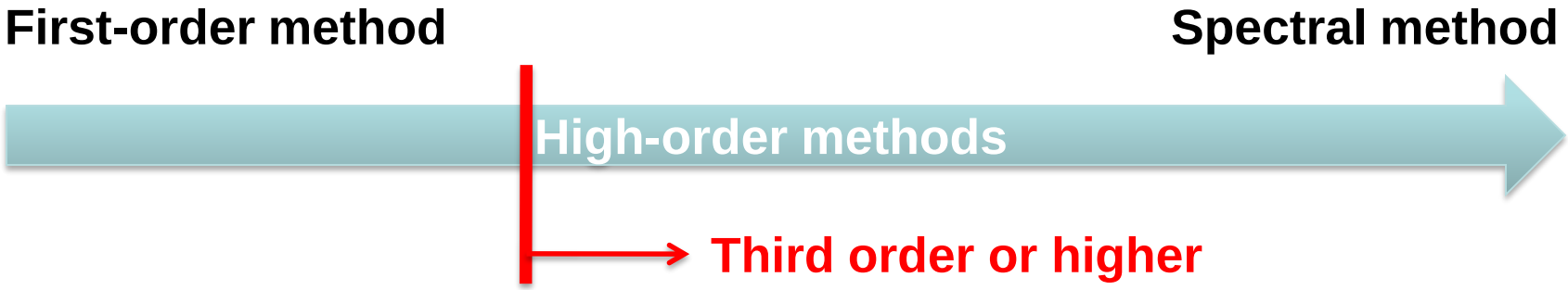

*** Z. J. Wang et al., High-Order CFD Methods: Current Status and Perspective, Int. J. Numer. Meth. Fluids, 2012.**

Why they are currently rarely used?

- More complicated than low-order methods
- Less robust and slower to converge to steady state due to the reduced numerical dissipation
- A high memory requirement for implicit time stepping
- Robust high-order mesh generators not readily available
- Research investment by the CFD community from the 70s and the 90s made second-order methods efficient and robust

Why they are important?

- **High-order methods are needed to accurately resolve vortex dominated flows, aeroacoustics, LES, DNS, boundary-layer stability and transition, etc**

- **High-order methods have the potential in delivering numerical solutions of higher accuracy**

- **High-order methods are not necessarily expensive**

Methods for flows with strong shock

- **Shock capturing schemes have inherent problems with strong shock such as shock-turbulence problems and hypersonic boundary-layer stability since**
  - **DNS of turbulent flows require non-dissipative schemes which will give spurious oscillations around shocks.**
  - **Traditional shock-capturing schemes are dissipative around shock which are not suitable for simulations of turbulent flow.**
  - **Extreme grid stretching is needed near the strong shock**

- **Relevance of Shock-fitting schemes:**
  - **Shock is treated sharply by shock-fitting schemes hence no grid stretching is required.**
  - **Shock-fitting is valid when shock thickness is much smaller than the smallest length associated with turbulence which is proved to be true for Mach 3 and stronger shocks.**

→ **High-order shock-fitting methods for hypersonic flow**

Governing equations for hypersonic flow

$$\frac{\partial \rho_s}{\partial t}+\frac{\partial}{\partial x_j}(\rho_s u_j)-\frac{\partial}{\partial x_j}(\rho D_s \frac{\partial y_s}{\partial x_j})=\omega_s$$

$$\frac{\partial}{\partial t}(\rho u_i)+\frac{\partial}{\partial x_j}(\rho u_i u_j+p\delta_{ij})-\frac{\partial}{\partial x_j}\left[\mu\left(\frac{\partial u_i}{\partial x_j}+\frac{\partial u_j}{\partial x_i}\right)-\frac{2}{3}\mu\frac{\partial u_k}{\partial x_k}\delta_{ij}\right]=0$$

$$\frac{\partial \rho E}{\partial t}+\frac{\partial}{\partial x_j}(\rho H u_j)-\frac{\partial}{\partial x_j}\left[u_i\mu\left(\frac{\partial u_i}{\partial x_j}+\frac{\partial u_j}{\partial x_i}\right)-\frac{2}{3}u_i\mu\frac{\partial u_k}{\partial x_k}\delta_{ij}\right]$$

$$-\frac{\partial}{\partial x_j}\left(\rho\sum_{s=1}^{5}h_s D_s\frac{\partial y_s}{\partial x_j}\right)-\frac{\partial}{\partial x_j}\left(K\frac{\partial T}{\partial x_j}+K_V\frac{\partial T_V}{\partial x_j}\right)=0$$

$$\frac{\partial \rho e_V}{\partial t}+\frac{\partial}{\partial x_j}(\rho e_V u_j)-\frac{\partial}{\partial x_j}(\rho\sum_{s=1}^{5}h_{V,s}D_s\frac{\partial y_s}{\partial x_j})-\frac{\partial}{\partial x_j}\left(K_V\frac{\partial T_V}{\partial x_j}\right)$$

$$=\sum_{s=1}^{3}Q_{T-V,s}+\sum_{s=1}^{5}\omega_s e_{V,s}$$

$$\frac{\partial U}{\partial t}+\frac{\partial F_j}{\partial x_j}+\frac{\partial F_{vj}}{\partial x_j}=0$$

$$F_j=\begin{Bmatrix}\rho u_j\\ \rho u_1 u_j+P\delta_{1j}\\ \rho u_2 u_j+P\delta_{1j}\\ \rho u_3 u_j+P\delta_{1j}\\ (e+p)u_j\end{Bmatrix}$$

$$F_{vj}=\begin{Bmatrix}0\\ -\tau_{1j}\\ -\tau_{2j}\\ -\tau_{3j}\\ -\tau_{jk}u_k+q_j\end{Bmatrix}$$

- **Two temperature model**
  - **Translation temperature (T) : Translation energy and rotation energy**
  - **Vibration and electron temperature (Tv): Vibration energy and electron energy**
  - **Three modules: perfect gas, 5-species air, and 11-species air**

Shock-fitting: perfect gas flow

To Find: $H(\xi,\eta,\zeta,\tau)$ $H_\tau(\xi,\eta,\zeta,\tau)$

$$\eta(x,y,z,t)=\eta_{\max}=\text{constant} \qquad v_n=-\frac{\eta_t}{|\nabla\eta|}$$

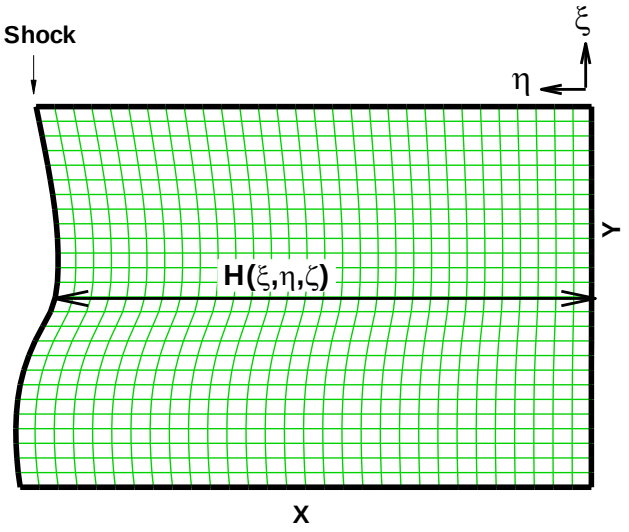

Time derivative of Rankine-Hugoniot Relations

$$[\mathbf{F}']=(\mathbf{F}_s-\mathbf{F}_0).\mathbf{a}+(U_s-U_0).\eta_t/J=0$$

$$\mathbf{a}=\frac{\eta_x}{J}\hat{i}+\frac{\eta_y}{J}\hat{j}+\frac{\eta_x}{J}\hat{k}$$

$$\partial[\mathbf{F}']/\partial\tau=0$$

+

Compatibility Equation

$$\mathbf{I}_N.\mathbf{B}_s'=\frac{|\nabla\eta|}{J}(u_n-v_n+c)_s\,\mathbf{I}_N, \quad \mathbf{B}_s'=\partial\mathbf{F}_s'/\partial\mathbf{U}$$

$$\frac{\partial}{\partial\tau}\left(\frac{\eta_t}{J}\right)=\frac{-1}{\left[\mathrm{I_N}\cdot(\mathrm{U_s}\text{-}\mathrm{U_0})\right]}\left[\frac{|\nabla\eta|}{J}(u_n-v_n+c)\mathrm{I_N}\cdot\left(\frac{\partial\mathrm{U}}{\partial\tau}\right)_s+\mathrm{I_N}\cdot(\mathbf{F_s}\text{-}\mathbf{F_0})\cdot\frac{\partial\mathbf{a}}{\partial\tau}-\mathrm{I_N}\cdot\left(\frac{\partial\mathbf{F_0}}{\partial\tau}\cdot\mathbf{a}+\frac{\partial\mathrm{U}_0}{\partial\tau}\cdot b\right)\right]$$

$$\frac{\partial H_\tau}{\partial\tau}=f\left(\xi,\zeta,\mathbf{U_s},\mathbf{I_N}\cdot\left(\frac{\partial\mathbf{U}_s}{\partial\tau}\right),\mathbf{U}_0,\left(\frac{\partial\mathbf{U}_0}{\partial\tau}\right),H,H_\tau\right)$$

$$\frac{\partial H}{\partial\tau}=H_\tau$$

High-order schemes for flow after shock

- **Spatial discretization**

Upwinding scheme

$$\left(\frac{\partial \psi}{\partial \eta}\right)_i = \frac{1}{h b_i}\sum_{j=-3}^{3} a_{i+j}\psi_{i+j} - \frac{\beta}{6! b_i} h^5 \left(\frac{\partial^6 \psi}{\partial \eta^6}\right)_i + \cdots \qquad with \quad \beta < 0$$

Central scheme

$$\left(\frac{\partial^2 \psi}{\partial \eta^2}\right)_i = \frac{1}{90 h^2}\sum_{j=-3}^{3} l_{i+j}\psi_{i+j}$$

Fourier collocation method for spanwise flux derivatives

- **Temporal integration** $\dfrac{d\vec{U}}{dt} = f\left(\vec{U}\right) + g\left(\vec{U}\right)$

$$\begin{cases} \vec{k}_1 = h\left[f\left(\vec{U}^n\right) + g\left(\vec{U}^n + a_1\vec{k}_1\right)\right] \\ \vec{k}_2 = h\left[f\left(\vec{U}^n + b_{21}\vec{k}_1\right) + g\left(\vec{U}^n + c_{21}\vec{k}_1 + a_2\vec{k}_2\right)\right] \\ \vec{k}_3 = h\left[f\left(\vec{U}^n + b_{31}\vec{k}_1 + b_{32}\vec{k}_2\right) + g\left(\vec{U}^n + c_{31}\vec{k}_1 + c_{32}\vec{k}_2 + a_3\vec{k}_3\right)\right] \\ \vec{U}^{n+1} = \vec{U}^n + \omega_1\vec{k}_1 + \omega_2\vec{k}_2 + \omega_3\vec{k}_3 \end{cases}$$

Order of accuracy evaluation I

(shock-entropy wave interaction – similar to Shu-Osher problem)

For $x < x_0$

$$\rho = (\gamma+1)M^2 \Big/ \left[(\gamma-1)M^2+2\right]$$

$$u = \gamma^{1/2}\left[2\left(M^2-1\right)\Big/\left\{(\gamma+1)M\right\}-M\right]$$

$$p = 1+2\gamma\left(M^2-1\right)\Big/(\gamma+1)$$

Freestream wave:

$$\rho_\infty = 1.0+\varepsilon\sin^4\left\{2.5\pi\left(x+M\gamma^{1/2}t\right)\right\}$$

$$u_\infty = -M\gamma^{1/2}$$

$$p_\infty = 1.0$$

Where, $\gamma = 1.4, M = 3, \varepsilon = 0.2, x_0 = 2.0$

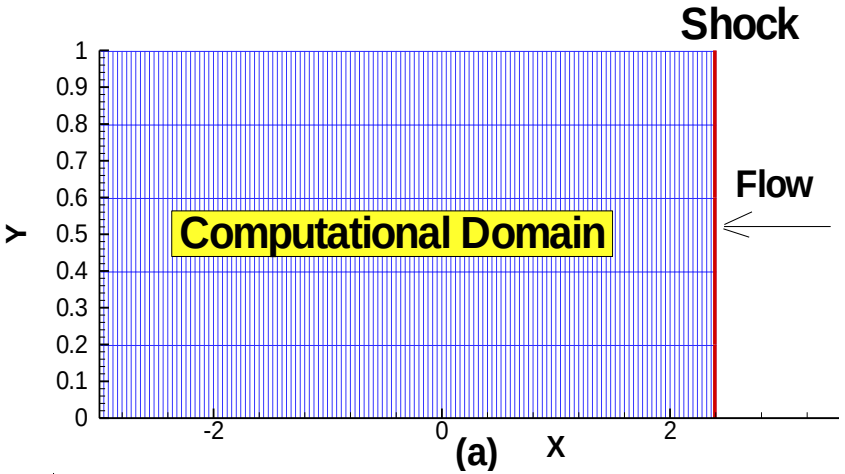

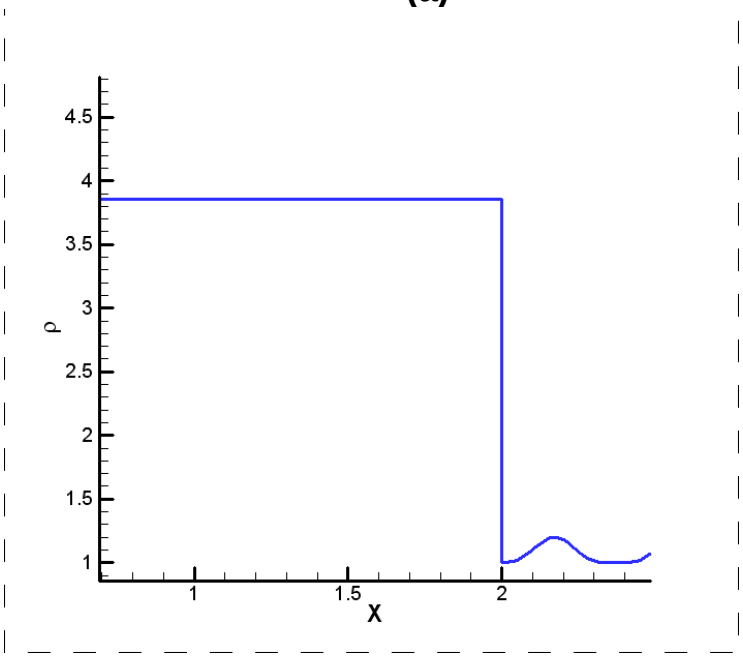

- **This problem is suitable for convergence study as there is not a sudden jump in density and upto 3rd order spatial derivatives of density profile are smooth.**

Order of accuracy evaluation II

(shock-entropy wave interaction – similar to Shu-Osher problem)

Grid-set 1: Spacing, $dx_1 = 2.5 \times 10^{-3}$

Grid-set 2: Spacing, $dx_2 = 1.25 \times 10^{-3}$

Grid-set 3: Spacing, $dx_3 = 6.25 \times 10^{-4}$

Order $$n = \log\left(\frac{e_{\Delta x}}{e_{\Delta x/2}}\right) \Big/ \log(2)$$

L-1 errors

	Error I:	Error II:	Error III:	Order from I and II	Order from II and III
Density	1.02E-05	4.39E-07	1.63E-08	4.5412991	4.747224
Velocity	7.77E-07	2.43E-08	7.89E-10	4.99887	4.94489
Pressure	5.87E-06	1.89E-07	6.06E-09	4.958014	4.961402

* Pradeep, S. R., *Simulations of Turbulent Flow Interactions with Strong Shocks Using Shock-Fitting Methods*, Dissertation of University of California, Los Angeles, 2010.

Order of accuracy evaluation III

(shock and vorticity-entropy wave interaction)

Perturbations :

$$u' = U_1 A_v \sin\psi_1 \cos(k_x x + k_y y - U_1 k_x t)$$

$$v' = -U_1 A_v \cos\psi_1 \cos(k_x x + k_y y - U_1 k_x t)$$

$$\rho' = \rho_1 A_e \cos(k_x x + k_y y - U_1 k_x t)$$

$$p' = 0$$

$$A_v = A_e = 0.025$$

$$k_y = k \sin\psi_1 = 1$$

$$k_x = k \cos\psi_1 \quad with \quad k = 1$$

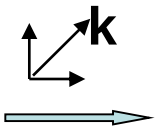

Mach 1.5 Mean Flow + Vorticity wave disturbance

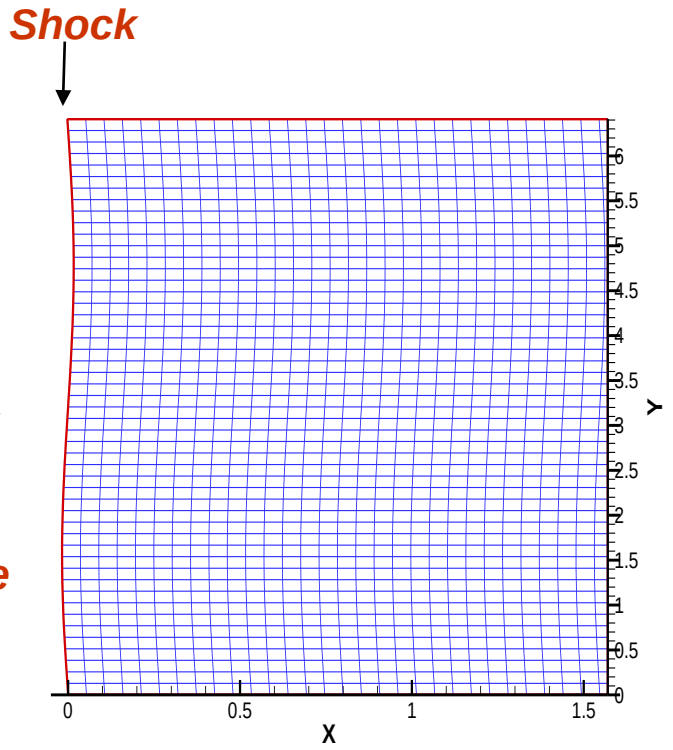

To Solve this problem with conventional shock-fitting:

- Shock is treated as boundary of the domain
- Fluctuations are superimposed just upstream of the shock .
- Periodic conditions are used in the direction parallel to the steady shock.
- Non reflecting boundary conditions are used at subsonic exit.

Order of accuracy evaluation IV

(shock and vorticity-entropy wave interaction)

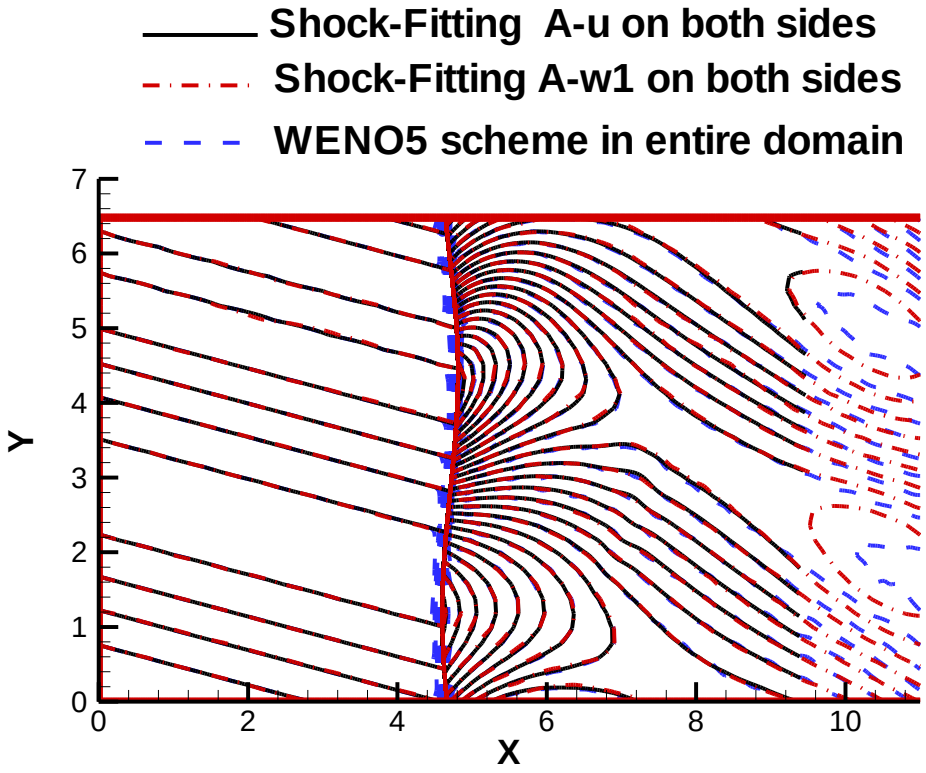

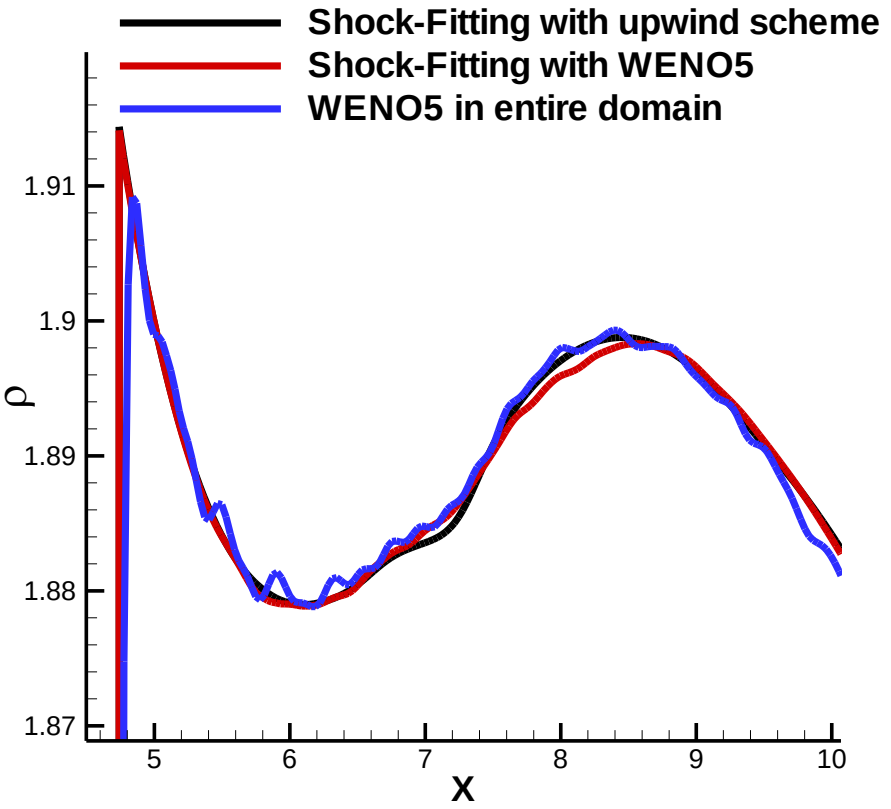

Comparisons of various schemes for incident wave coming in at 75 degree angle of incidence: shock-fitting algorithm works much better

* Pradeep, S. R., *Simulations of Turbulent Flow Interactions with Strong Shocks Using Shock-Fitting Methods*, Dissertation of University of California, Los Angeles, 2010.

Shock-fitting: non-equilibrium flow

➢ Shock-fitting algorithm

- **Species concentrations keep constant across the shock**
- **Shock jump conditions**
- **One compatibility relation from behind the shock, corresponding to the eigenvalue (U+a)**

$$R=\begin{bmatrix} a^2\delta_{sr}-c_s\tilde{\gamma}_r & \beta u c_s & \beta v c_s & \beta w c_s & -\beta c_s & -\phi c_s \\ -\tilde{V} & l_x & l_y & l_z & 0 & 0 \\ -\tilde{W} & m_x & m_y & m_z & 0 & 0 \\ \tilde{\gamma}_r-\tilde{U}a & an_x-\beta u & an_y-\beta v & an_z-\beta w & \beta & \phi \\ \tilde{\gamma}_r+\tilde{U}a & -an_x-\beta u & -an_y-\beta v & -an_z-\beta w & \beta & \phi \\ -e_V\tilde{\gamma}_r & \beta u e_V & \beta v e_V & \beta w e_V & -\beta e_V & a^2-\phi e_V \end{bmatrix}$$

$$\begin{cases} \dfrac{\partial H_\tau}{\partial \tau}=f\left(\xi,\zeta,\vec{U}_s,\mathrm{I_N}\cdot\left(\dfrac{\partial \vec{U}}{\partial \tau}\right)_s,\vec{U}_\infty,\dfrac{\partial \vec{U}_\infty}{\partial \tau},H,H_\tau\right) \\ \dfrac{\partial H}{\partial \tau}=H_\tau \end{cases}$$

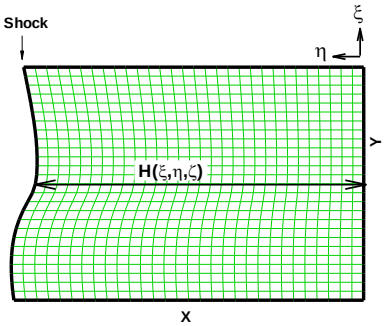

Test 1: Air flow over a 1 meter cylinder

(Shock-fitting solver vs LAURA)

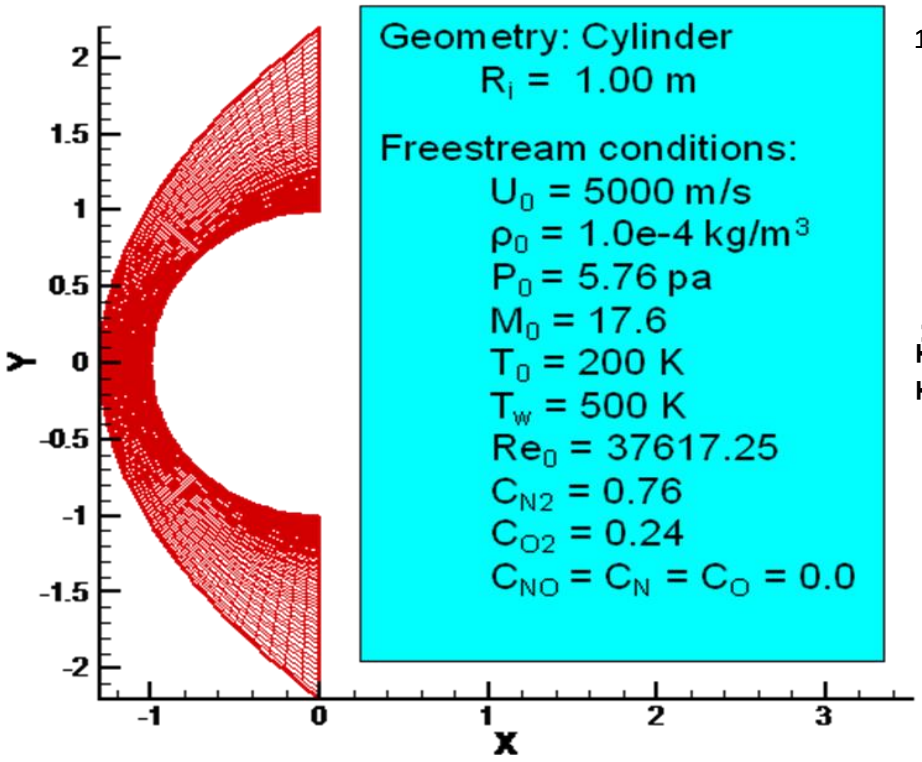

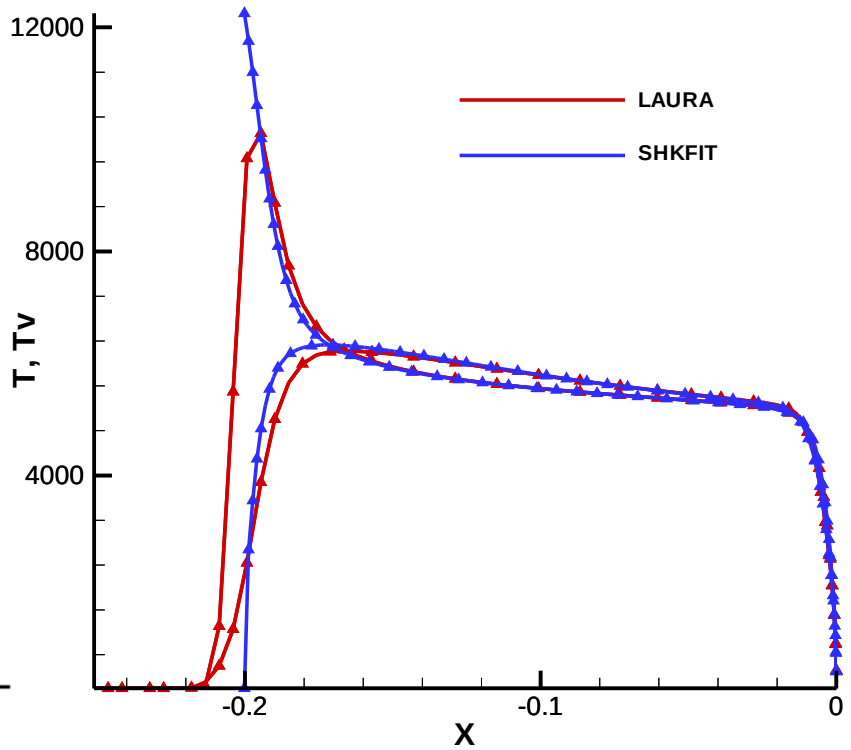

- Solution of Gnoffo is obtained using LAURA code, where vibration and electron energy is obtained from curve fits.
- The grid used in our simulation is exactly the same as that used by Gnoffo.
- Shock-fitting result has a good agreement with Gnoffo's, except near the shock.

Test 1: Air flow over a 1 meter cylinder

(Shock-fitting solver vs LAURA)

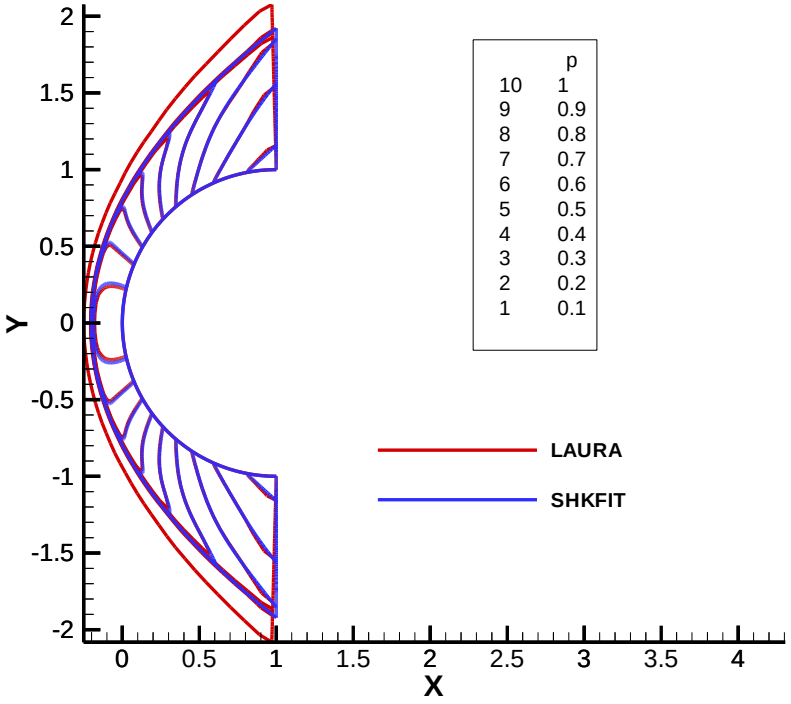

Pressure

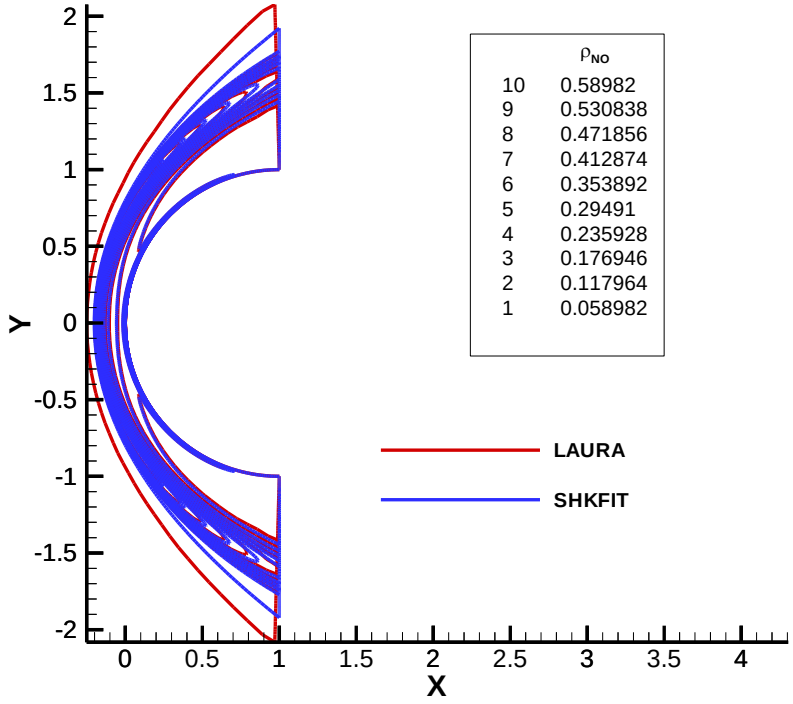

Mass fraction of NO

Test 2: A Mach 11.18 flow over a sphere

(Shock-fitting solver vs US3D)

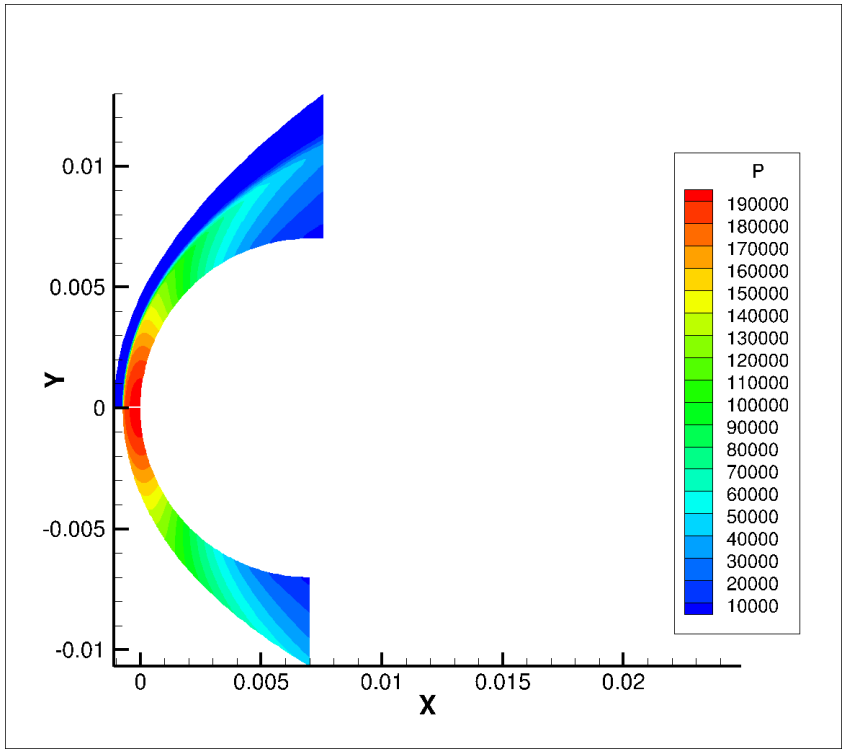

Pressure

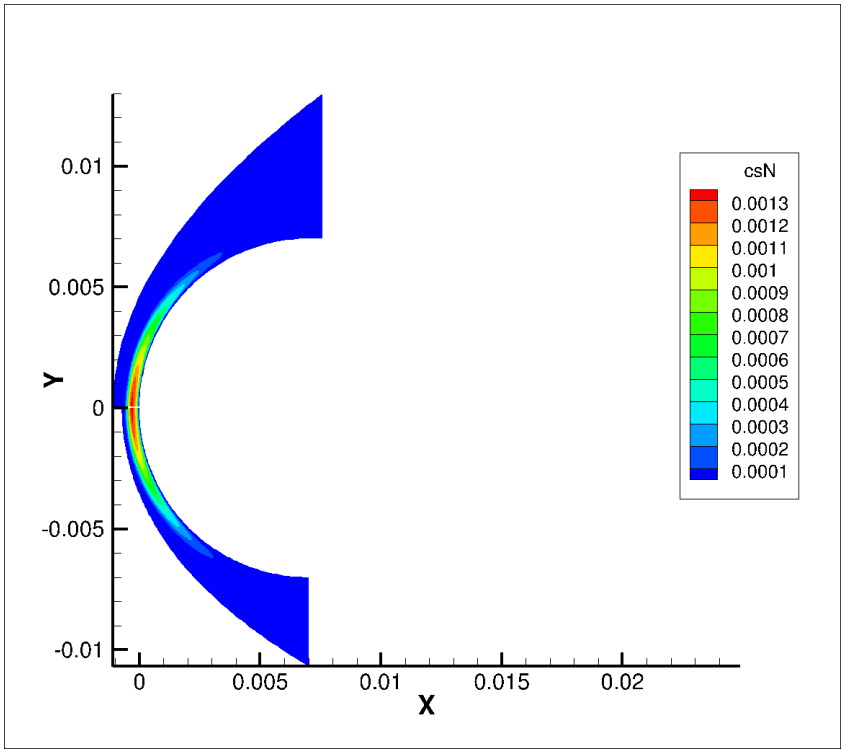

Mass fraction of N

Case No.	Code	M_∞	U_∞ m/s	T_∞ K	P_∞ pa	h0 MJ/kg	T_w K	Re_∞ ($\times 10^6$) 1/m	Radius mm	Medium
1	SHKFIT	11.18	3844	293	1200	7.68*	1000	2.83*	7 7 ° cone	Air/N_2

Chart of previous research topics

Computational Fluid Dynamics

Development of high-order numerical methods

Hypersonic boundary-layer stability and transition path

DNS of strong shock and turbulence interaction

Transition control
- **Surface porous coating**
- **Discrete and/or continuous surface roughness (patented)**

Collaboration on theoretical analysis

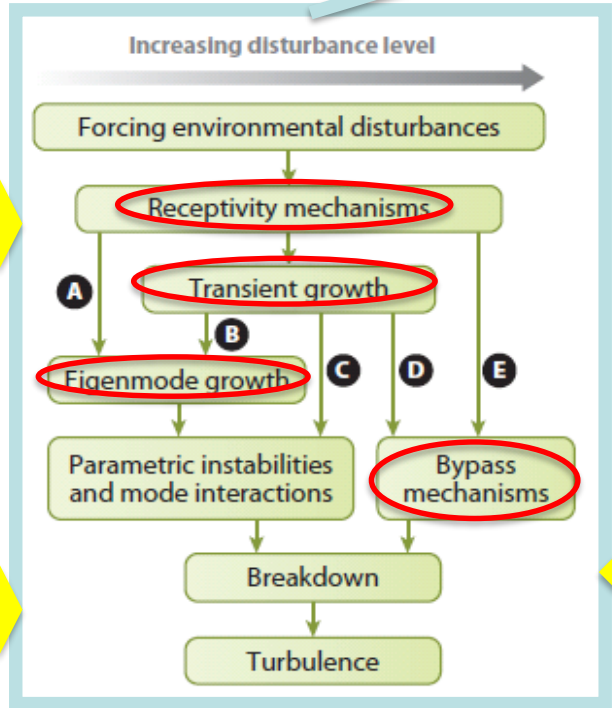

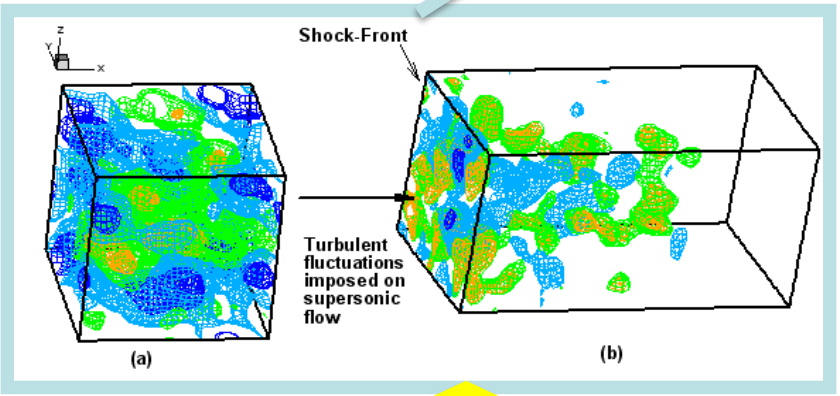

Effects of thermochemical non-equilibrium on high temperature flows behind strong shocks
- **Two-temperature model**
- **State-by-state kinetic model**

Stability of Mach 8 flow to blow suction

n	$f_n^*(kHz)$	$\omega_n^*(kHz)$	$F_n \times 10^6$
1	14.92	93.74	9.63
2	29.84	187.48	19.26
3	44.76	281.23	28.89
4	59.68	374.97	38.52
5	74.60	468.71	48.15
6	89.52	562.45	57.78
7	104.44	656.19	67.41
8	119.36	749.94	77.04
9	134.28	843.68	86.67
10	149.20	937.42	96.30
11	164.12	1031.16	105.93
12	179.04	1124.91	115.56
13	193.96	1218.65	125.19
14	208.88	1312.39	134.82
15	223.80	1406.13	144.45

➢ Flow conditions

$$M_\infty = 8.0\,, \qquad T_\infty^* = 54.78\,K\,,$$
$$p_\infty^* = 389Pa\,, \qquad Pr = 0.72\,,$$
$$Re_\infty^* = \rho_\infty^* U_\infty^* / \mu_\infty^* = 8.2 \times 10^6/m\,.$$

➢ Blowing-suction models

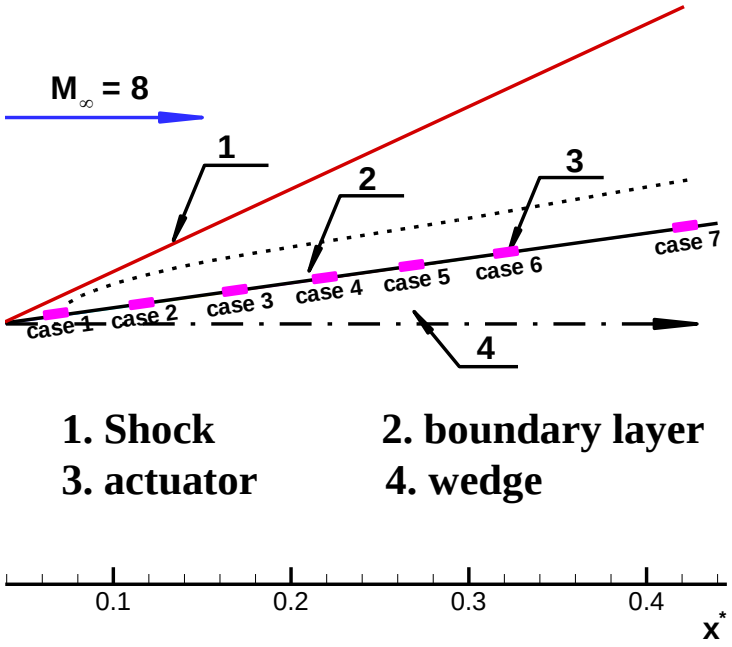

1. Shock **2. boundary layer**
3. actuator **4. wedge**

Features of hypersonic boundary layer

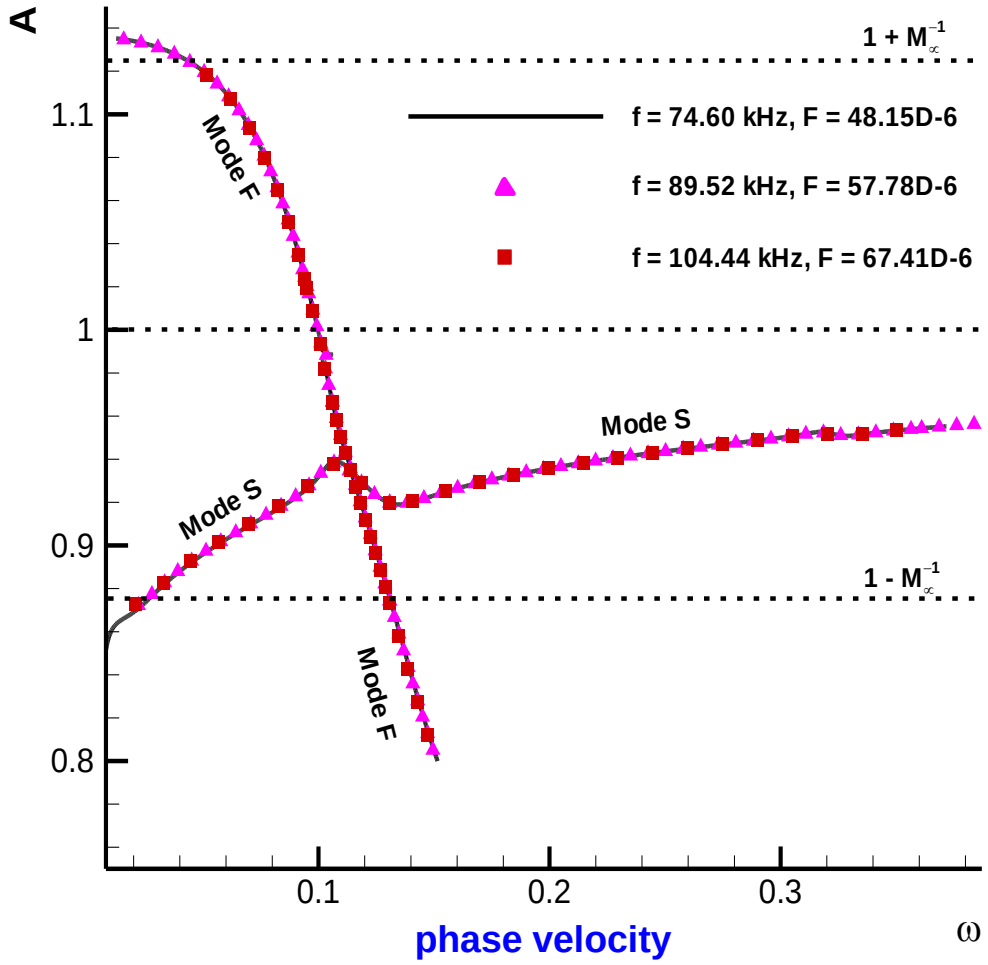

phase velocity

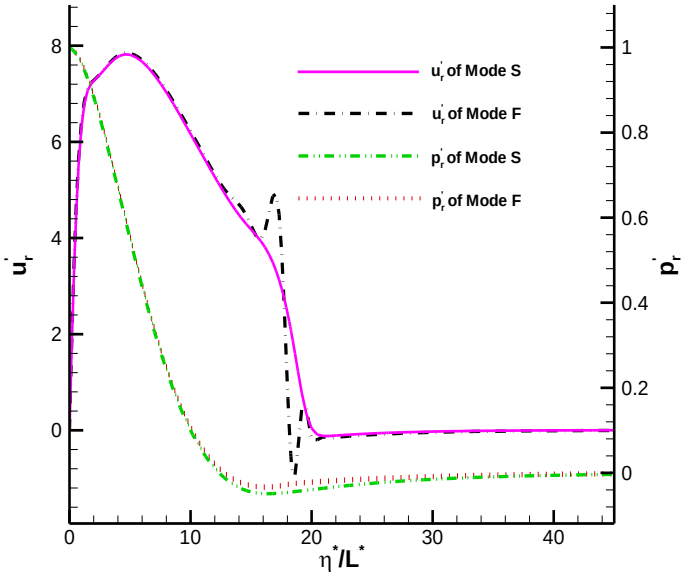

eigenfunction comparison of mode S and mode F at synchronization point

- Phase velocities are almost independent of frequency.
- Mode S and mode F have the same phase velocities and similar eigenfunctions at the synchronization point $\omega_S = 0.11443$.
- The synchronization point are as follows:

$$s^*_{sn} = \frac{(\omega_s/F_n)^2}{Re_\infty}$$

Perturbations at fixed frequency I

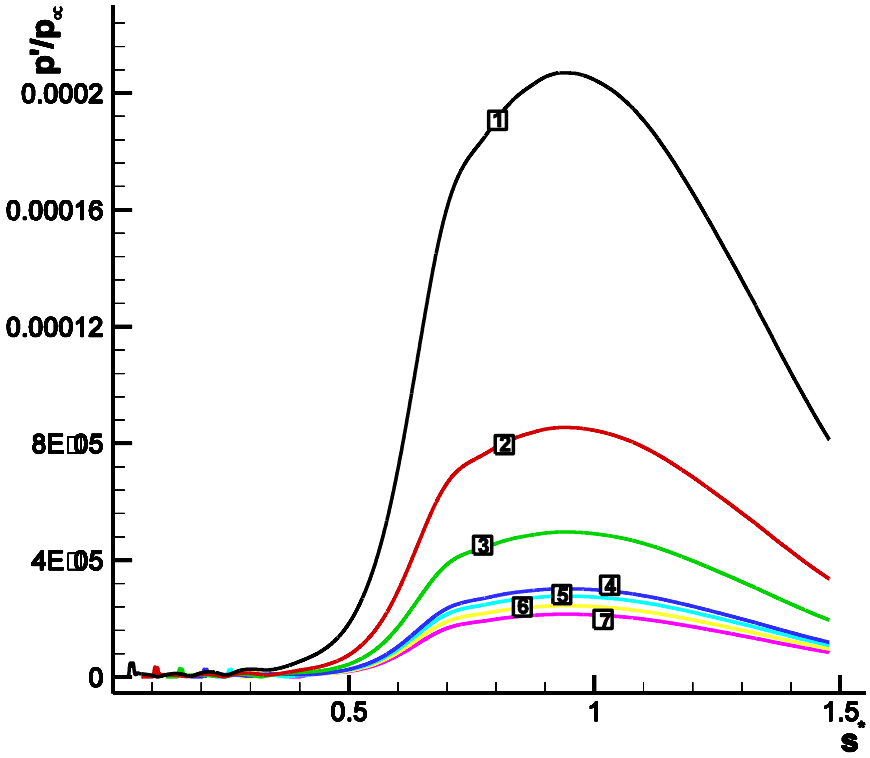

f_6 = 89.52 kHz, S_{syn} = 0.4719m

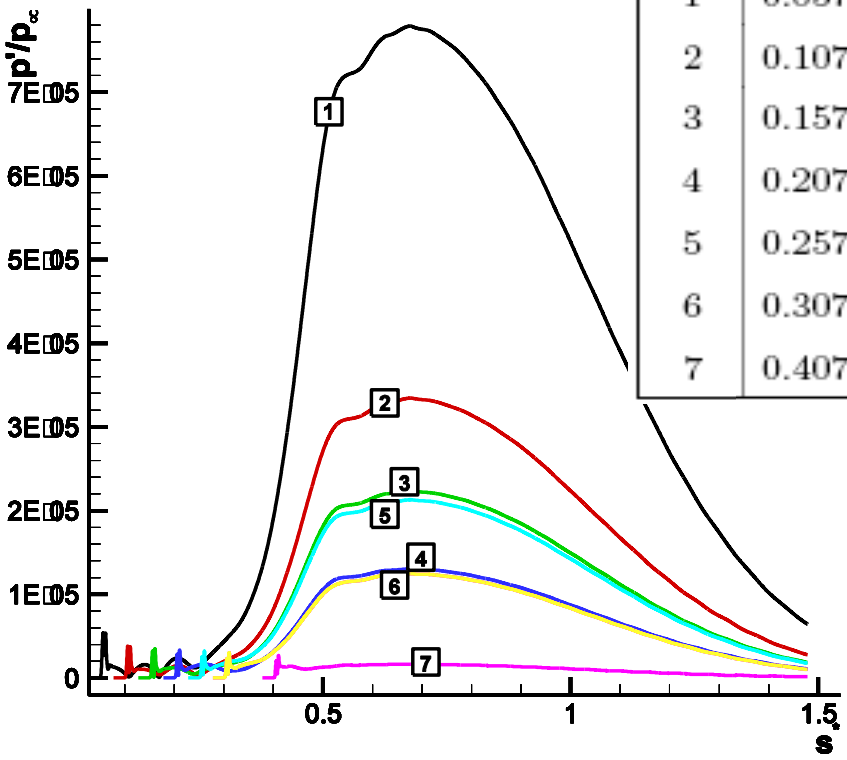

case	s_c^* (m)
1	0.05784
2	0.10784
3	0.15784
4	0.20784
5	0.25784
6	0.30784
7	0.40784

f_7 = 104.44 kHz, S_{syn} = 0.3467m

Perturbations at fixed frequency II

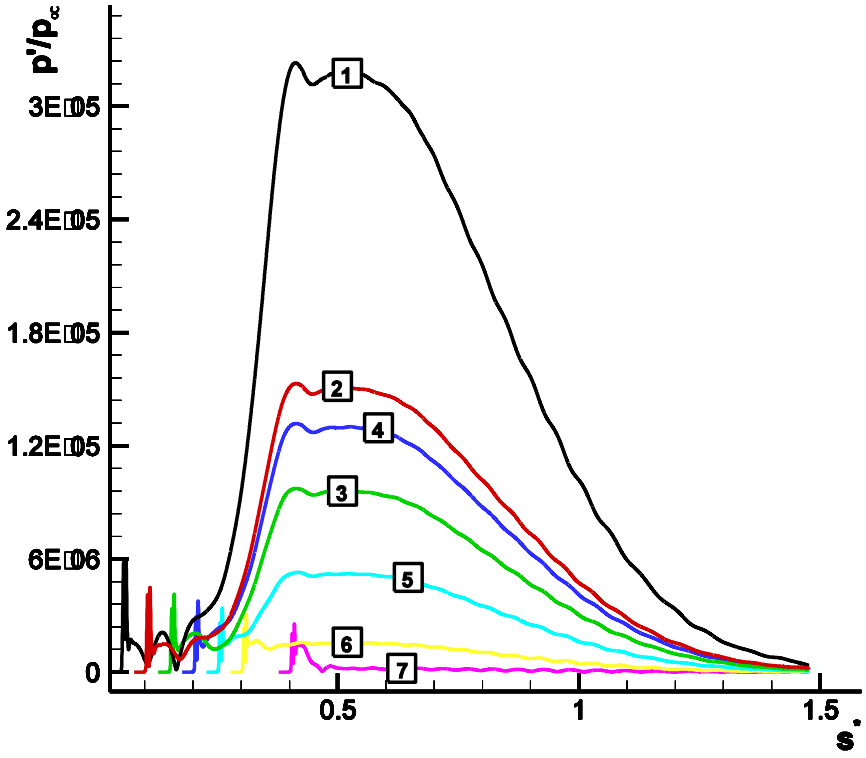

f_8 = 119.36 kHz, S_{syn} = 0.2654m

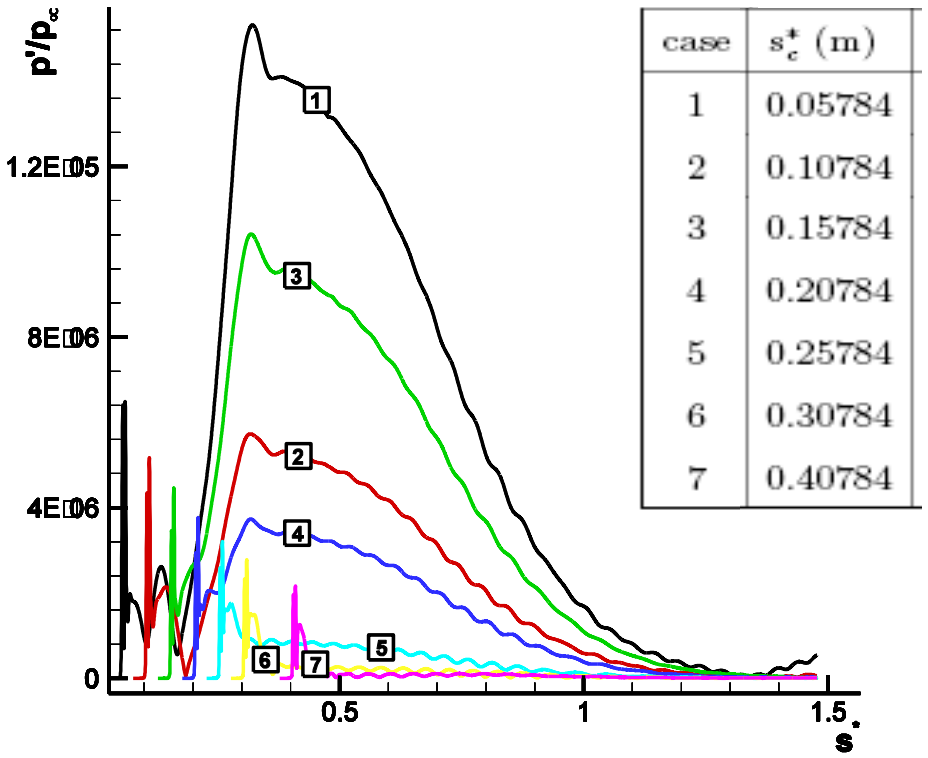

case	s_c^* (m)
1	0.05784
2	0.10784
3	0.15784
4	0.20784
5	0.25784
6	0.30784
7	0.40784

f_9 = 134.28 kHz, S_{syn} = 0.2097m

Hint from the results

- **The synchronization point plays an important role in the excitation of mode S by the blowing-suction actuator.**

- **The relationship between the location of blowing-suction actuator and the synchronization point indicates: in order to control or delay the laminar-turbulent transition with wall blowing-suction, the blowing-suction actuator should be located upstream of the synchronization point.**

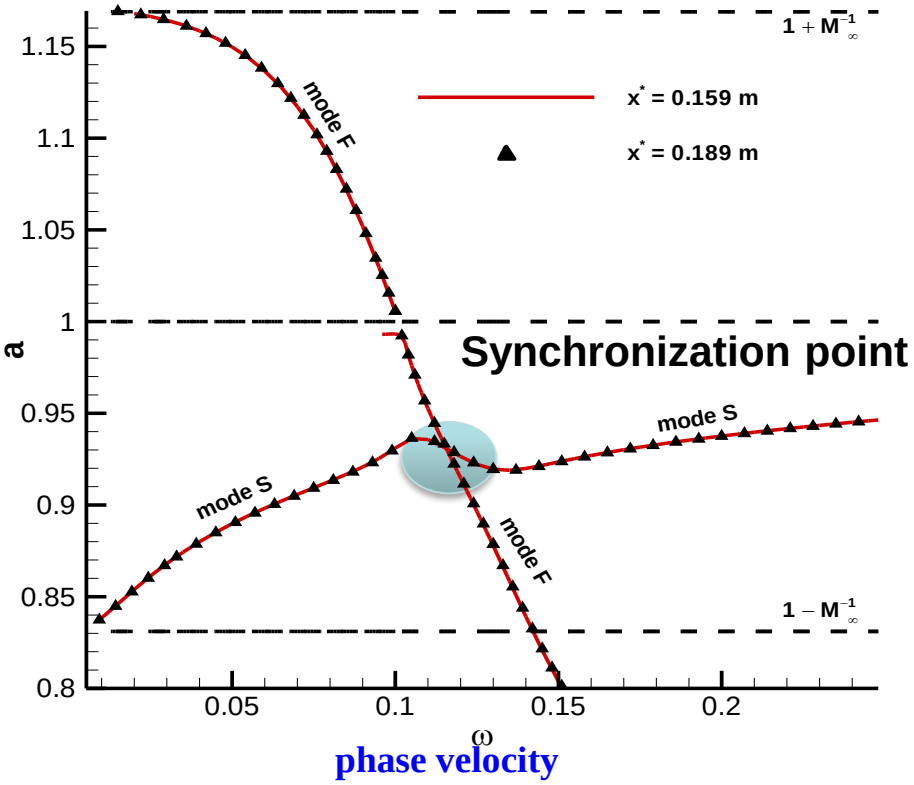

Flow stabilization using roughness

➢ Flow conditions

$M_\infty = 5.92$ $\quad T_\infty = 48.69\,\mathrm{K}$

$p_\infty = 742.76\,\mathrm{Pa}$ $\quad \mathrm{Pr} = 0.72$

$\mathrm{Re}_\infty = 13\times10^6/\mathrm{m}$

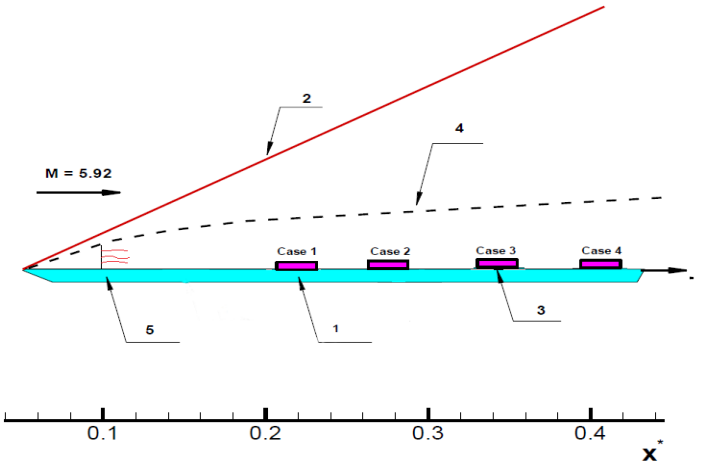

➢ Disturbance at the inlet

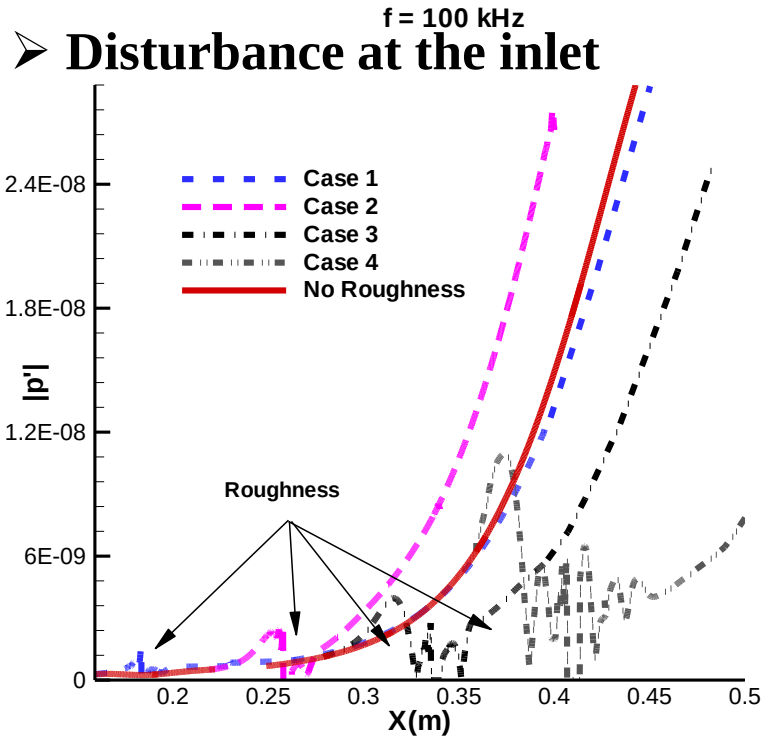

$$\begin{Bmatrix}\tilde{u}\\ \tilde{v}\\ \tilde{w}\\ \tilde{p}\\ \tilde{T}\end{Bmatrix} = \varepsilon \begin{Bmatrix}\hat{u}(y)\\ \hat{v}(y)\\ \hat{w}(y)\\ \hat{p}(y)\\ \hat{T}(y)\end{Bmatrix} \sin(\omega t)$$

➢ **RHS disturbance vector represents the eigenfunction of a specific boundary-layer wave (100kHz).**

The growth of pressure perturbation

- The roughness location (0.185 m) corresponds to the synchronization point at 133.26 KHz.
- 120 KHz perturbation is amplified by roughness (The roughness is before the synchronization point).
- Both 130 KHz and 140 KHz perturbations are damped by roughness (The roughness is after the synchronization point).

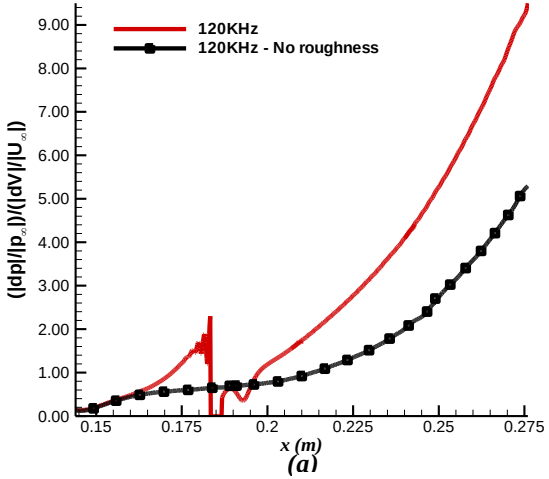

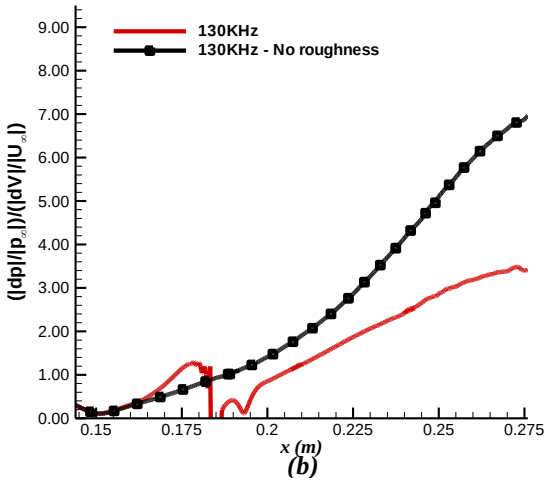

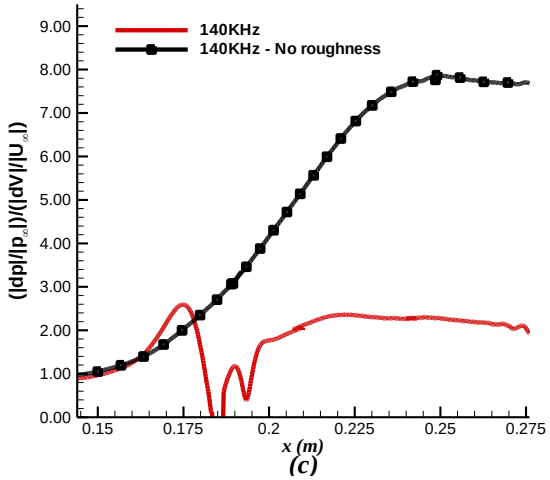

What about two roughness elements?

- **Roughness spacing is about 10 roughness width. First roughness location: 133.26 KHz. Second roughness location: 119.26 Khz.**
- **120 KHz perturbation is amplified by the first roughness since it is locates upstream of its sync pt. However, it is damped by the second roughness since the second roughness is close to its sync pt.**
- **Both roughness are located at or downstream of the sync point of 130 KHz and 140 KHz perturbations. Therefore, the disturbances of these two frequencies are damped by both roughness.**

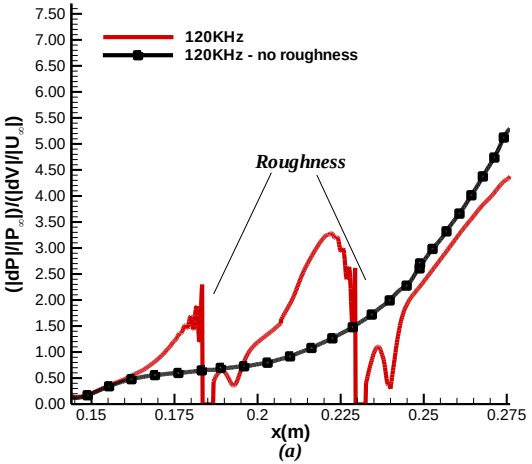

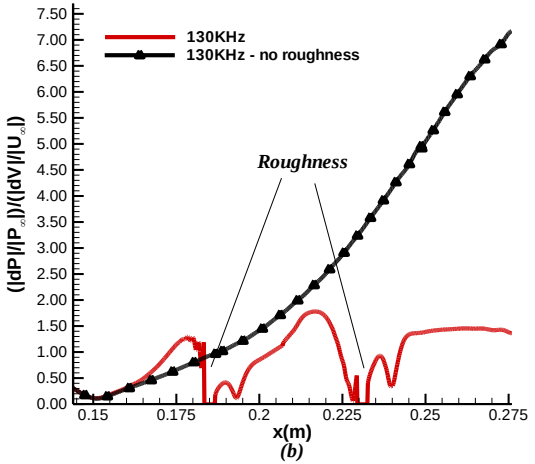

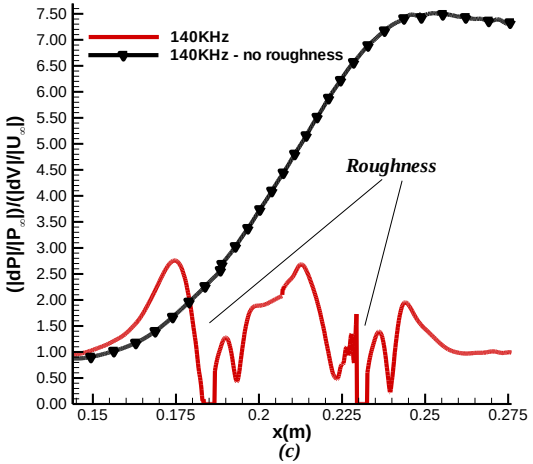

Test of simulation and experiment

Flow conditions

Re^*_∞	$1.026 \times 10^7\ m^{-1}$
P^*_o	965 kPa ≈ 140 psia
T^*_∞	52.8 K
T^*_o	433.0 K
T^*_{wall}	300.0 K
ρ^*_∞	$0.0403\ kg/m^3$
γ	1.4
Pr	0.72
R^*	287.04 N·m / kg·K (air)
μ^*_r	1.7894×10^{-5} kg / m·s (sea level)
T^*_r	288 K (sea level)
T^*_s	110.3 K

UCLA designed roughness

Roughness #	S (m) (center of roughness)	x (m) (center of roughness)	Roughness height (mm)	Roughness width (mm)
1	0.3	0.2985	0.665	2.66
2	0.3266	0.3226	0.665	2.66
3	0.3532	0.3503	0.665	2.66
4	0.3798	0.3783	0.665	2.66
5	0.4064	0.4045	0.665	2.66
6	0.433	0.4298	0.665	2.66

Purdue model

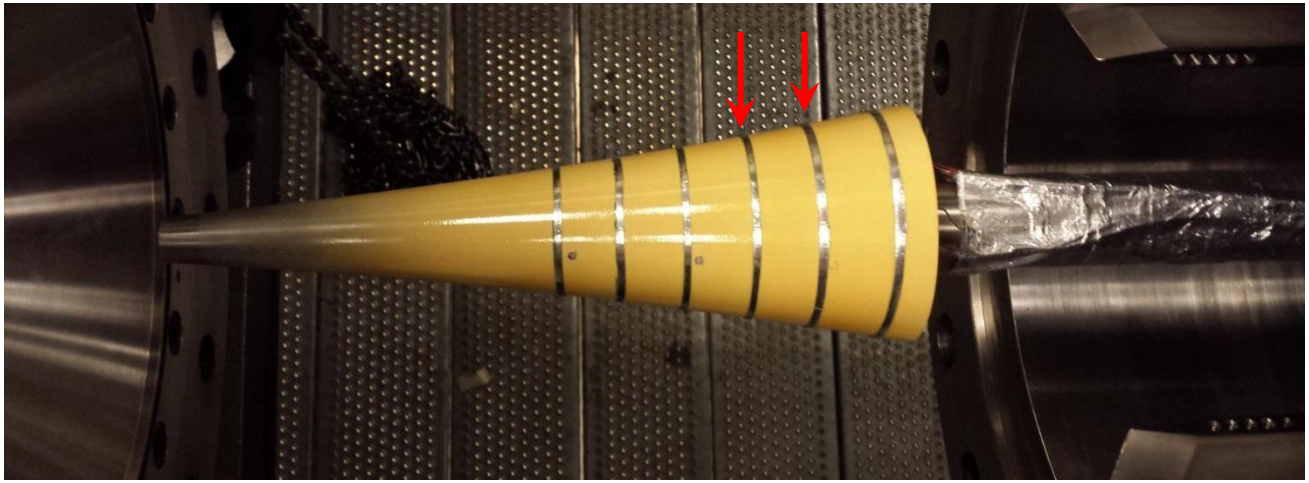

Experiment of roughness effect

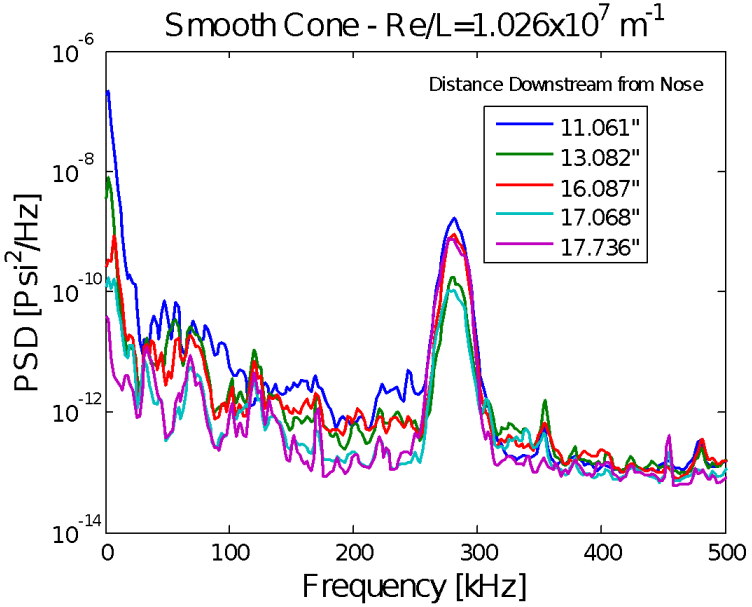

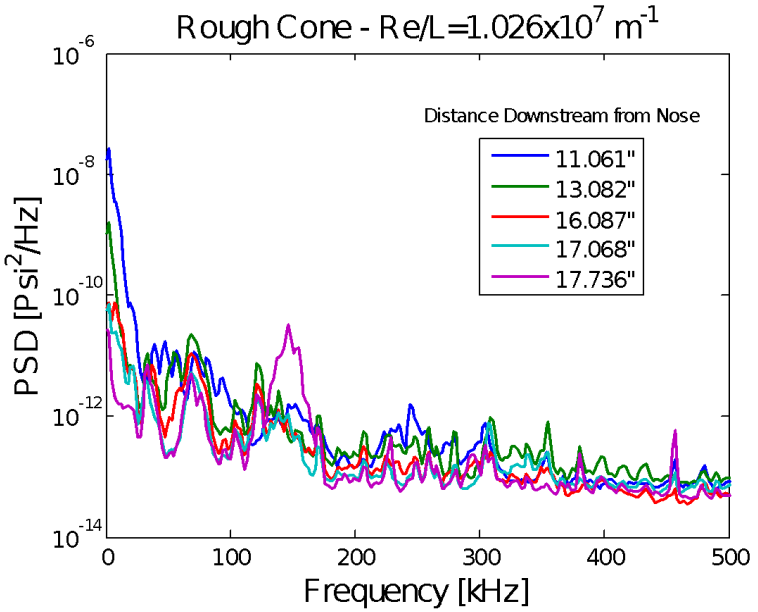

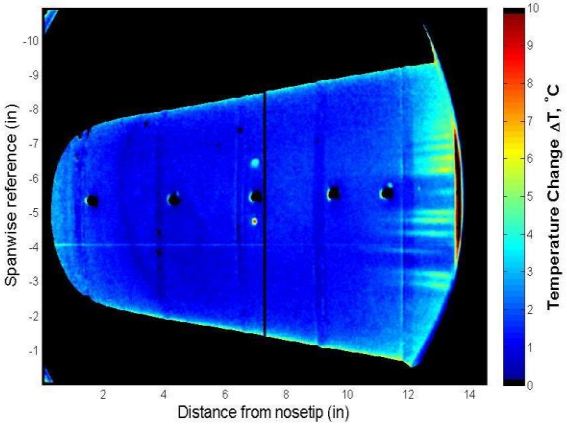

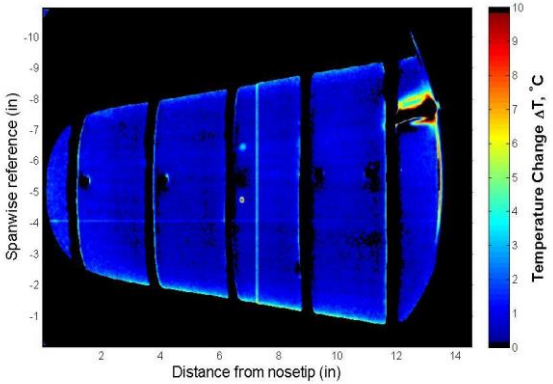

Patent: Hypersonic laminar flow control

- The control of laminar flow can be achieved by applying an array of surface roughness elements in the region before the laminar-turbulent transition.
- The roughness elements may have a height between 40% and 60% of the local boundary-layer thickness.
- The exact location, height, and spacing of surface roughness elements may be determined by a numerical simulation strategy based on the most unstable second mode, e.g. using known e^N transition prediction method, experimental measurement, or any other suitable technique.

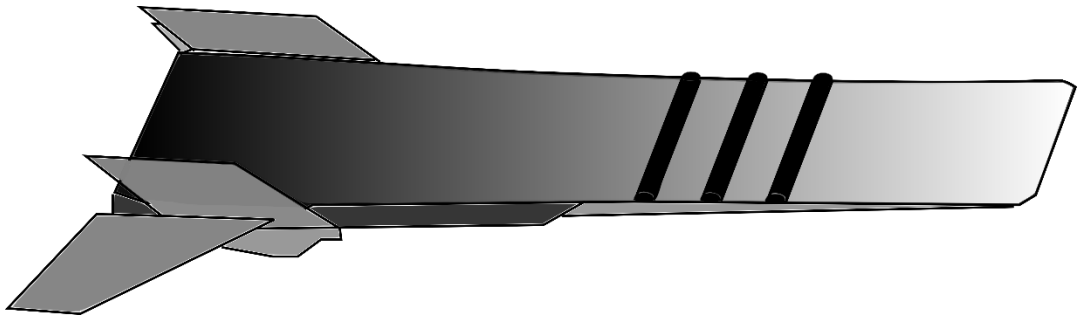

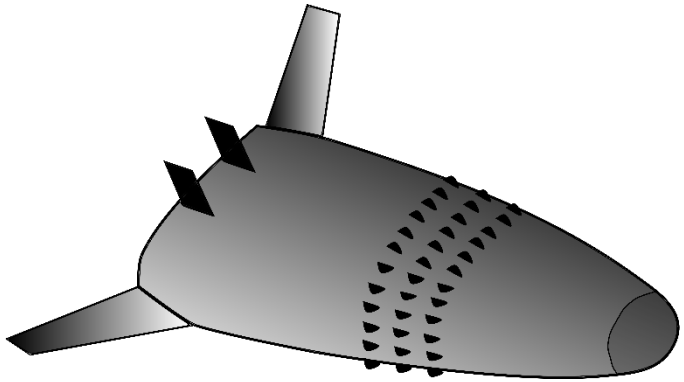

*** https://www.google.com/patents/US20150336659**

Simulations of thermal protect system

- Some thermal protection systems (TPS) of hypersonic vehicles are ablative such as may be found on reentry vehicles
- Boundary layer transition strongly influences heat transfer to the vehicle so its prediction is critical when sizing TPS
- TPS is commonly overdesigned because boundary layer prediction is difficult which increases the vehicle weight
- There exists little numerical work on surface chemistry or ablation effects on hypersonic boundary layer transition

Copyright Space X

- Develop and verify a module of the high-order shock-fitting method with a surface chemistry model for thermal protection system

Numerical simulations of sonic boom

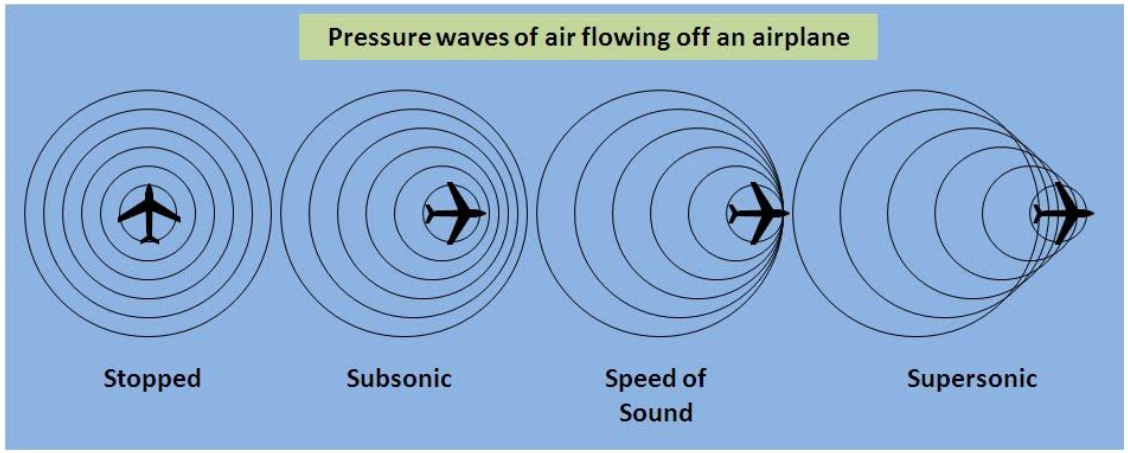

Formation of sonic boom

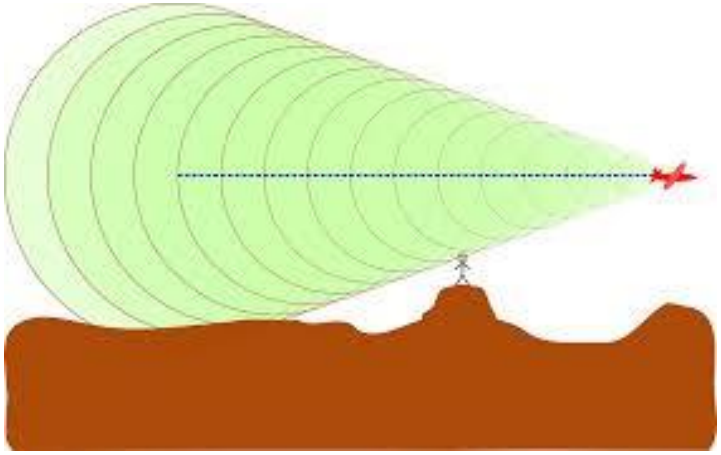

Sonic boom in real life

- For supersonic flight, noise (acoustics) combines into shock wave, the classic “Boom! Boom!” signature
- Due to the annoying sonic boom, commercial supersonic flight over land are currently prohibited.
- Numerical simulations are needed for the design of faster supersonic jet which may even include non-equilibrium effects.

NASA & Lockheed Martin: QueSST

DNS of shock and turbulence interaction

- **Interactions of turbulent flows and shock waves are important in many natural processes as well as scientific and engineering applications where very high rates of compression and expansion waves are generally observed**
  - Volcanic eruption
  - Supernova explosion
  - Detonation
  - High-speed aerodynamics
  - Shock wave lithotripsy to break up kidney stones
  - Energy of inertial confinement fusion

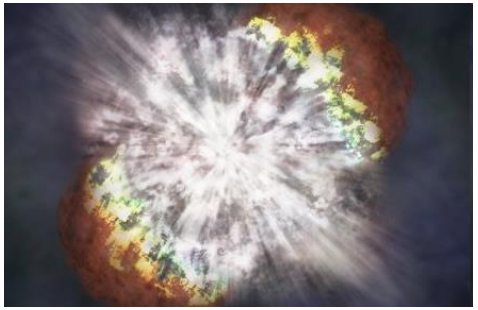

- **One of the fundamental building blocks in these complex processes and applications is the canonical problem of interaction of isotropic turbulence and a normal shock**

- **The underlying physics in strong shock and turbulence interaction is essential for better understanding of such processes and applications.**

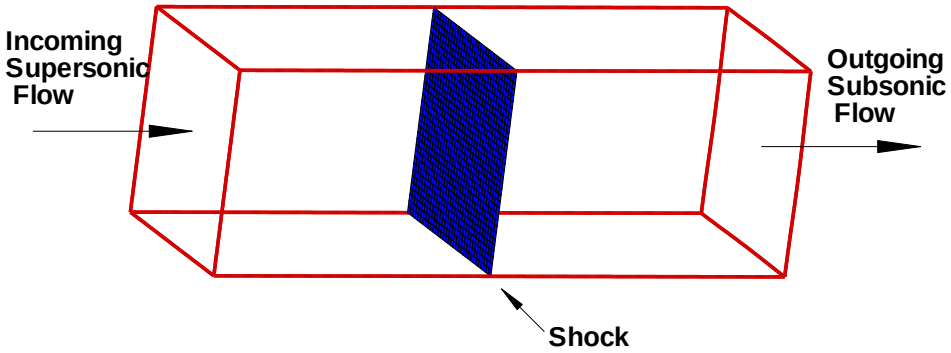

Typical schematic of isotropic shock and turbulence interaction problem

Summary

- **Compared with low order CFD method, high-order methods are quite important due to its capability to achieve high-order accuracy**

- **A high-order shock-fitting method has been developed and verified for numerical simulations of high-speed/non-equilibrium flows which includes different modules for different problems**

- **The application of the high-order shock-fitting method leads to the patent of hypersonic laminar flow control – delay laminar-turbulent transition by appropriately designed surface roughness**

- **The high-order shock-fitting method can be applied to internal flow simulations as well as external flow simulations, such as thermal protection system, low boom supersonic jet, flows around high-speed flight vehicles and through their propulsion systems, DNS of turbulent flow interacting with strong shocks, etc.**